Article

Optical Properties of Valve Metals Functional Thin Films Obtained by Electrochemical Anodization on Transparent Substrates

Liudmila S. Khoroshko [1,2,*] **, Aleksey V. Baglov** [1,2] **, Taisa I. Orekhovskaya** [2] **, Sergei V. Trukhanov** [3,4] **, Daria I. Tishkevich** [3,5] **, Alex V. Trukhanov** [3,4] **, Tamara F. Raichenok** [6] **and Anatoly I. Kopots** [2]

1 Faculty of Physics, Belarusian State University, 4 Nezavisimosti Av., 220030 Minsk, Belarus
2 R & D Department, Belarusian State University of Informatics and Radioelectronics, P. Brovki Str. 6, 220013 Minsk, Belarus
3 Laboratory of Magnetic Films Physics, SSPA "Scientific and Practical Materials Research Centre of NAS of Belarus", P. Brovki Str. 19, 220072 Minsk, Belarus
4 Smart Sensors Laboratory, National University of Science and Technology MISiS, 119049 Moscow, Russia
5 Laboratory of Single Crystal Growth, South Ural State University, Lenin Ave. 76, 454080 Chelyabinsk, Russia
6 Center "Photonics of Atomic and Molecular Structures", Stepanov Institute of Physics, National Academy of Sciences of Belarus, 220072 Minsk, Belarus
* Correspondence: l.s.khoroshko@gmail.com; Tel.: +375-17-293-53-59

Abstract: Nanostructured aluminum, tantalum, and vanadium oxide layers on glass substrates were obtained by electrochemical anodizing in oxalic and sulfuric–oxalic electrolytes. The morphological and optical properties of the obtained structures were investigated experimentally by scanning electron microscopy and transmission spectroscopy. Obtained oxide coatings are quasi-ordered arrays of vertical (aluminum oxide/tantalum oxide, aluminum oxide/vanadium oxide, and aluminum oxide obtained in the oxalic electrolyte) or non-ordered tree-like (aluminum oxide obtained in the sulfuric–oxalic electrolyte) pores depending on the initial film metal and anodizing technology. The light transmission in the range of 750–1200 nm is up to 60% for aluminum oxide/tantalum oxide/glass (annealed) and quasi-ordered aluminum oxide/glass structures, and around 40% for aluminum oxide/tantalum oxide/glass (not annealed) and aluminum oxide/vanadium oxide. Non-ordered aluminum oxide is characterized by low transmission (no more than 8%) but has a developed surface and may be of interest for the formation of films with poor adhesion on smooth substrates, for example, photocatalytic active xerogels. The refractive indices of dispersion of the obtained layers were calculated from the transmission spectra by the envelope method. The dispersion of the refractive indices of the obtained oxide films is insignificant in a wide range of wavelengths, and the deviation from the average value is assumed to be observed near the intrinsic absorption edges of the films. The glasses with proposed semi-transparent nanostructured oxide layers are promising substrate structures for subsequent sol–gel coating layers used in photocatalytic purification systems or up-conversion modules of tandem silica solar cells with forward and reverse illumination.

Keywords: valve metals oxides; porous anodic films; transmission spectra; refractive index; transparent substrates; nanostructured oxide layers

1. Introduction

Multilayer oxide and semiconductor films of nanostructured materials on optically transparent substrates are currently being actively studied for optics and microelectronics applications as interference filters, for controlling the absorption and reflection coefficients of semi-transparent structures, elements of conducting electrodes, hydrophobic coatings, as well as for the formation of the optically active material on them, including the possibility of obtaining nanostructured film scintillators with improved characteristics in the pores [1–7].

Nanostructured oxides of valve metals can be obtained by electrochemical anodizing in acidic and alkalic electrolytes with the possibility of controlling the geometrical parameters of oxide films by electrolyte concentration and temperature, anodic current and voltage, etc. While the anodic oxidation of aluminum leads to Al_2O_3 amorphous oxide forms, vanadium and tantalum anodic oxides consist of non-stoichiometric chemical compounds Ta_xO_y (or V_xO_y), which during heat treatment are oxidized to higher oxides with known optical, physical, and chemical properties [8–12].

The formation of anodic films on transparent substrates has been of interest to many research groups in recent years [13–20]. Most of the provided experiments focused on obtaining oxides on glasses as intermediate materials for further use as substrates for xerogels, conductive electrodes, templates for the synthesis of nanopillars, etc. [17–21]. The production of anodic oxide on the dielectric glass substrate is associated with several difficulties. Therefore, in most cases, glasses with conductive coatings are used, such as, for example, ITO/glass structure. Anodizing aluminum on such a conductive substrate is simpler, but the conductive layer may later turn out to be redundant for some applications. Moreover, the preparation of conductive coatings on glasses increases the complexity of creating the final structure. In most cases, to obtain an ordered structure, anodization of aluminum layers occurs in two stages, or the finished oxide is exposed to additional chemical etching to expand the mouths of the pores. Both of those methods have limits. So, the two-stage process requires more thickness from initial films, but sputtering processes may not always provide sufficient adhesion and formation of an integral layer, which can lead to the undesirable formation of multilayer films. Figure 1 represents, for example, an anodic aluminum oxide film obtained from sputtered 5 μm film on a Si substrate.
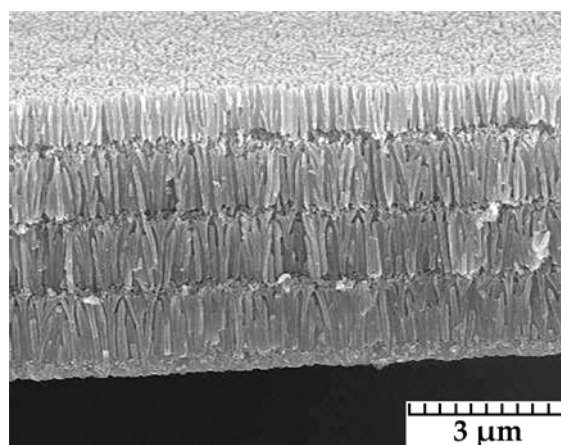

Figure 1. Cross-section of the aluminum oxide anodic film obtained in 1 M phosphoric acid at 100 V from 5 μm Al film on a Si substrate.

Chemical etching of the anodic films bears the risk of removing oxide layers from the substrate as well as violating the porosity and integrity of the walls of the cell pore. We propose to consider the possibility of creating translucent anode layers of valve metals on substrates by a one-stage anode process without additional chemical treatment after anodizing.

Submicron layers of porous anodic aluminum oxide (PAAO) on transparent substrates make it possible to provide the necessary adhesion to the films obtained by the sol–gel method and form luminescent or photocatalytic structures on their basis [3,4] while maintaining a sufficient degree of light transmission in a given wavelength range. The PAAO is possessed of the high reactivity outer layer of the porous anodic oxide, which is due to the residues of organic compounds, the presence of –OH groups, and the developed porous surface of the oxide. These properties are important for obtaining coatings on PAAO by chemical methods such as deposition, immersion, sol–gel, etc. In turn, the formation of PAAO on nanometer layers of tantalum or vanadium provides sufficient adhesion of the

porous layer to a smooth substrate and makes it possible to form large-area films. The transmittance degree and refractive index are important parameters of the coatings for optical applications, both single-oxide and combined.

In general, anodic aluminum oxide is transparent to visible and infrared light, with its transparency dependent on several factors, including the thickness of an anodic layer, concentration and type of impurities, and the diameter and ordering of pores [22–25]. The best results show highly ordered structures, which can be obtained, at the simplest level, by two-stage anodizing [22,24–28]. Thus, one of the main tasks is to find a balance between the complexity of the manufacturing technology and the required defect-freeness for high transparency in coatings.

Interesting properties of PAAO and other porous semiconductors are the phenomena of birefringence in a porous oxide, as in a disordered structure with anisotropy on the scale of the radiation wavelength, and an asymmetric light reflectance effect [29,30]. These underlie the prospects of using PAAO as a birefringent material in the optical region of the spectrum as a replacement for expensive, strictly ordered photonic crystal materials and natural crystals. PAAO has a large working surface area, the ability to control the magnitude of birefringence due to a controlled change in the geometry of the porous oxide, a relatively low cost, and relative ease of manufacturing [28].

In addition, one of the promising areas for using porous anodic oxides is as a host matrix or template for synthesizing composite materials, in particular nanowires, to obtain biocompatible structures and structures with special magnetic properties and surface characteristics [30–41].

This article presents the results of modifying the transmission degree and refractive index of glasses by forming micron layers of PAAO as well as combined oxide coatings from PAAO on submicron layers of semiconductor oxide compounds of vanadium and tantalum.

2. Materials and Methods

Porous anodic films were obtained on glass slides with dimensions of $26 \times 76 \times 1$ mm. Layers of initial metals were formed on glass substrates from high-purity (99.5%) vanadium and tantalum and high-purity (99.99%) aluminum metal sources on the 01-NE-7004 ORATORIYA-9 vacuum sputtering equipment (JSC "Kvartz", Kaliningrad, Russia). The following characteristics were implemented for technological processes of metal deposition: current 0.9 A, voltage 8 kV, sputtering time 7 min for Al; current 0.9 A, voltage 8 kV, sputtering time 2 min 40 s for Ta; current 0.4 A, voltage 8 kV, sputtering time 45 s for V. The thickness of the sublayer of Ta or V was 300 Å, while the thickness of the aluminum films was 1 μm.

Electrochemical oxidation of metal layers was carried out in potentiostatic mode in a solution of oxalic acid $H_2C_2O_4$ (0.3 mol/L) at a temperature of 6–7 °C, under a voltage of 60 V, as well as in a combined electrolyte containing 1.2 mol/L of sulfuric (H_2SO_4) and 0.6 mol/L of oxalic acid, at a temperature of 12 °C and a voltage of 20 V. All used reagents were of the chemical purity class. Distilled water was used for the preparation of electrolytes. Electrochemical oxidation was carried out over the entire thickness of the sputtered layers. After anodizing, the samples were dried at 100 °C in the air for an hour to remove physically bonded water and pre-oxidize tantalum and vanadium. We had assumptions that heat treatment could positively affect the transmission of structures. However, no significant effect was found. Registered changes in transmission were obtained only for the Al/Ta oxide structure after the annealing at 450 °C for 30 min, which is given in the article.

The morphological features of the obtained PAAO/oxide sublayer/glass structures were investigated by scanning electron microscopy (SEM) on a Hitachi S-4800 microscope (Hitachi High-Technologies Corporation, Tokyo, Japan). The transmittance and absorption spectra were measured on a Cary-500 Scan UV-VIS-NIR spectrophotometer (Varian, Melbourne, Australia).

The schemes of the experiment for the study of transparency are provided in Figure 2. For visually transparent samples, which we call "semi-transparent" below, the scheme from Figure 2a is used, and part Figure 2b represents the scheme for an "almost non-transparent" sample.
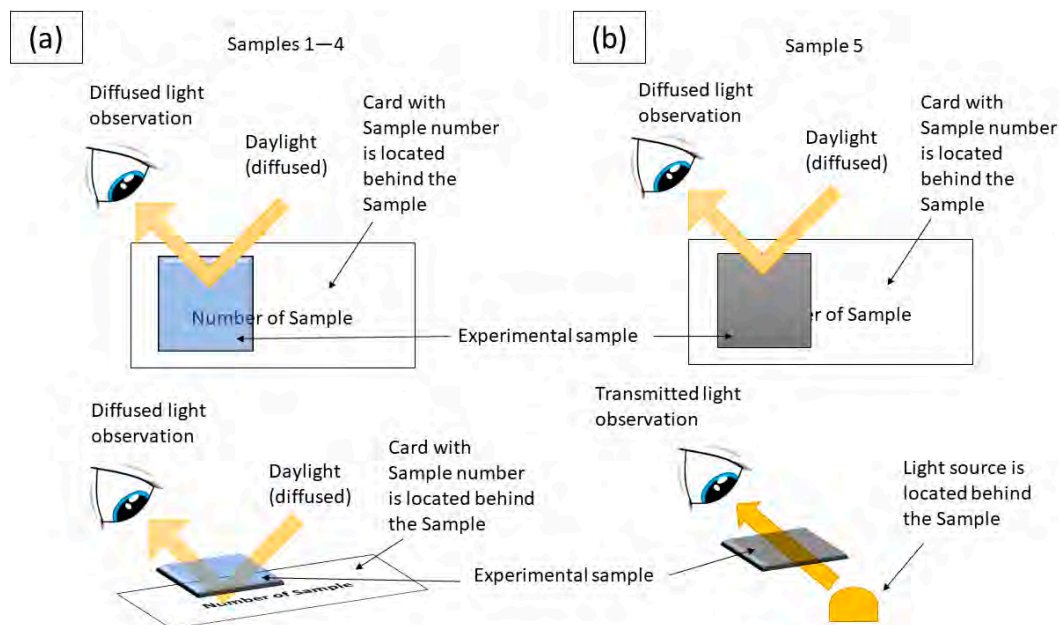

Figure 2. Schematic representation of experiments to evaluate the visual transmission of semi-transparent (**a**) and almost non-transparent (**b**) samples.

To assess the visual transparency, we placed a card with the sample number behind the sample (Figure 2a,b, top) and fixed the result with a portative 5 megapixel photo camera based on module K2A201E1CP (Samsung Electronics Co., Ltd., Suwon, South Korea). There are two variants of transparency when applying the sample to the card. It was possible to see the number on the card without additional light sources through samples 1–4 since these samples turned out to be sufficiently transparent (Figure 2a); the bottom shows the trimetric projection of the experiment, and the sample is raised for visibility, but during the experiment and photographing, the sample lay tightly on the card. The card was not visible through sample 5 in daylight (Figure 2b, top). When a light source was placed behind sample 5 (Figure 2b, bottom), it was possible to consider the oxide boundary and the presence of a light source. However, the photos with opposite lighting are not informative enough, and we do not provide them below.

3. Results and Discussion

According to the SEM analysis, PAAO has formed a quasi-ordered structure of vertical and tree-like pores arrays with a diameter of 20–30 nm depending on the anodizing mode, and the ordering of PAAO does not depend on the nature of the semiconductor sublayer. In Figures 3 and 4, SEM images of the structure of PAAO obtained in oxalic electrolytes and structures of Al/Ta and Al/V anodic oxides are represented.

Quasi-ordered aluminum oxide is a porous structure. The tantalum and vanadium oxide sublayers are formed as granular fragments repeating the pattern of the bottoms of the pores, and in addition, the granularity of the vanadium sublayer is less pronounced. The Al/Ta, Al/V, and aluminum oxides obtained in oxalic electrolyte films are visually transparent under daylight (on inserts in Figure 3a–d, figures with the sample numbers are placed behind them). According to SEM, the thickness of the anodic oxide sublayer of tantalum is 84 nm and that of vanadium is 70 nm. Considering that the layers of sputtered

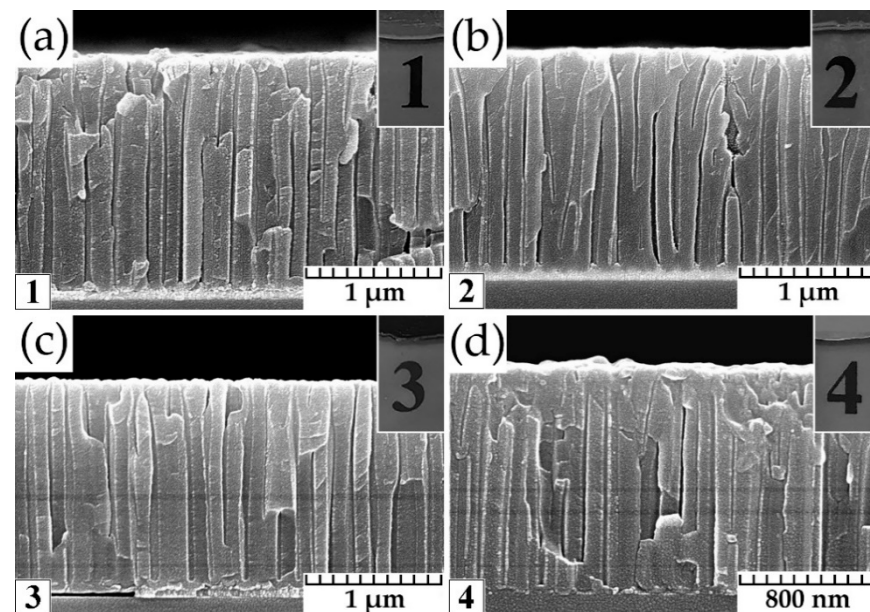Ta and V had the same thickness, we can assume the formation of a denser oxide in the case of vanadium.

Figure 3. SEM images of cross-sections of quasi-ordered valve metals functional thin films on the glass substrate (samples 1–4), and their photos in daylight (on inserts): (**a**) Al/Ta oxide; (**b**) Al/Ta annealed oxide; (**c**) Al/Va oxide; (**d**) Al oxide obtained in the oxalic electrolyte.
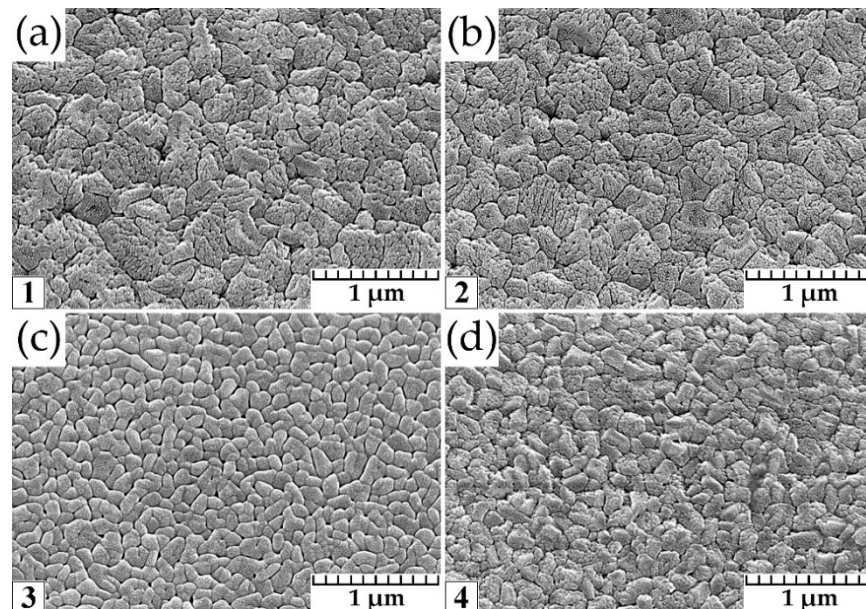

Figure 4. SEM images of surfaces of quasi-ordered valve metals functional thin films on the glass substrate (samples 1–4): (**a**) Al/Ta oxide; (**b**) Al/Ta annealed oxide; (**c**) Al/Va oxide; (**d**) Al oxide obtained in the oxalic electrolyte.

In contrast to the cross-section, for the surface, the influence of the electrolytes and sublayer on the structure is more pronounced (Figure 4).

The surfaces do not have an obvious ordered structure with pores of small diameter, which is due to the single-stage anodization. When carrying out a two-stage process, it is possible to obtain a surface with widened pore mouths, but this was not the goal of this synthesis. For the samples with Ta sublayer, a more enlarged domain structure

with pore mouths about 20 nm in diameter is observed (Figure 3a,b), and the samples without a sublayer have a more pronounced granularity of surface with about 20 nm mouth diameters (Figure 3d). The Al/V oxide layer is characterized by the smoothest surface, and the diameter of the pores reaches 30 nm, which makes it possible to form thin films with unexpressed relief on such samples without additional preparation. The developed surface of samples 1, 2, and 4 is a promising basis for the formation of films of materials for photocatalysis on them, as well as films with insufficient adhesion on smooth substrates.

Non-ordered PAAO is an array of tree-like pores with a pronounced granular barrier layer, and the oxide film is translucent only against the light (Figure 5, the insert in (a) demonstrates only a view of the sample under the experiment design from the top of Figure 2b). The surface of this sample is also characterized by granularity and narrow pores (about 10–20 nm).
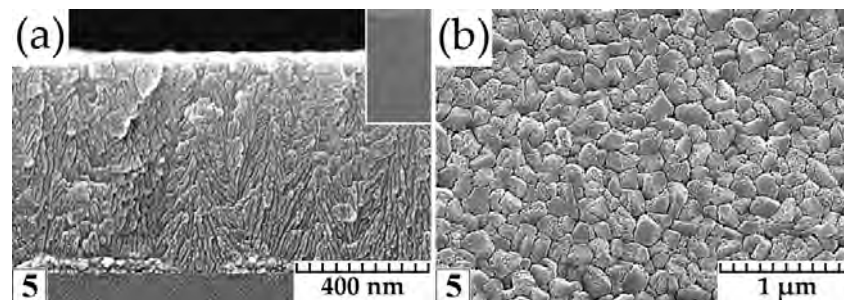

Figure 5. SEM image of the non-ordered anodic aluminum oxide film on the glass substrate obtained in the sulfuric–oxalic electrolyte (sample 5): (**a**) cross-section and photo transparency (insert); (**b**) surface.

At the same time, such a significant effect of the electrolyte as in the case of the cross-section is not observed, and the sulfuric–oxalic electrolyte shortens the anodizing time. The PAAO film formed in the combined electrolyte is the thinnest due to the higher dissolution rate in the combined electrolyte containing sulfuric acid [39,42,43]. In addition, the current density is much higher for anodization in combined electrolytes. In the presented experiment, the average current density in the oxalic electrolyte was about 4–6 mA/cm^2, and in the sulfuric–oxalic electrolyte, about 33 mA/cm^2. The maximum current density was observed during anodization in the oxalic electrolyte of the Al/V structure, which was also anticipated to affect its morphology (see Figures 2 and 3). Thus, the PAAO coating obtained in combined electrolytes could be recommended for non-optical use as a porous adhesion sublayer for the films. Summary information on the modes of obtaining and structural features of the samples is represented in Table 1.

Table 1. Composition, synthesis mode, and physical properties of investigated porous anodic oxide films.

Sample No.	Film Composition *	Anodizing Mode	Thermal Treatment	Orderliness of Porous Oxide	Refractive Index (Calculation)	Film Thickness, μm (Calculation)	Film Thickness, μm (SEM)
1	Ta_xO_y/Al_2O_3	0.3 M $H_2C_2O_4$, 60 V, 7 °C	100 °C, 30 min	quasi-ordered	1.526	1.98	1.82
2	Ta_xO_y/Al_2O_3	0.3 M $H_2C_2O_4$, 60 V, 7 °C	450 °C, 60 min	quasi-ordered	1.524	1.69	1.81
3	V_xO_y/Al_2O_3	0.3 M $H_2C_2O_4$, 60 V, 7 °C	100 °C, 30 min	quasi-ordered	1.521	1.98	1.68
4	Al_2O_3	0.3 M $H_2C_2O_4$, 60 V, 7 °C	100 °C, 30 min	quasi-ordered	1.521	1.45	1.33
5	Al_2O_3	1.2 M H_2SO_4 + 0.6 M $H_2C_2O_4$ 20 V, 12 °C	100 °C, 30 min	non-ordered	1.710	2.08	1.13

* Ta and V anodic oxides not specified.

The transmission spectra of the obtained oxide films on glass are shown in Figure 6. Alternations of minima and maxima are observed in the transmission spectra due to the interference of light in the quasi-periodic structure of the anodic oxide films. This characteristic of the transmission spectra makes it possible to determine the total refractive indices of oxide films, including combined oxide films, by the envelope method [5,44,45].
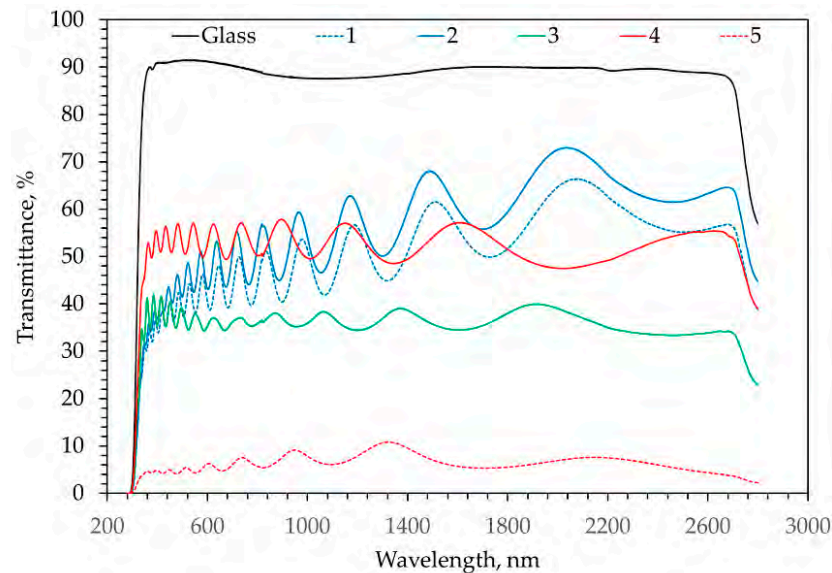

Figure 6. Transmission spectra of the valve metals functional thin films and the initial glass substrate.

In accordance with the envelope method, the maximum $T_{max}(\lambda)$ and the minimum $T_{min}(\lambda)$ in transmission spectra are determined to determine the values of the refractive index of the obtained films. The values of the transmittance coefficient on the envelope curves are obtained by parabolic extrapolation of experimentally determined points corresponding to the position of interference maxima and minima on the transmittance spectrum. Next, the refractive index of the film n is calculated according to the equation [45]:

$$n = [N + (N^2 - s^2)^{1/2}]^{1/2}, \tag{1}$$

where

$$N = [2s\,(T_{max}(\lambda) - T_{min}(\lambda))/T_{max}(\lambda)\,T_{min}(\lambda)] + (s^2 + 1)/2, \tag{2}$$

where s is the refractive index of the substrate (in this case, the refractive index is 1.51 for the used glass slides).

Based on the calculated refractive indices, it is possible to calculate the thickness of the studied coatings using the equation [45]:

$$d = A\,\lambda_1\,\lambda_2/2\,[n(\lambda_1)\,\lambda_2 - n(\lambda_2)\,\lambda_1], \tag{3}$$

where λ_1 and λ_2 are the wavelengths corresponding to adjacent extremes on the transmittance spectrum, the coefficient $A = 1$ for two adjacent extremes of the same type ($min - min, max - max$) and $A = 0.5$ for two adjacent extremes of the opposite type ($min - max, max - min$).

The results of the calculation for the studied films are represented in Table 1. As reference values, the thickness values obtained are used in SEM. The average discrepancy of the measurement results was about 10% for samples 1–4. Therefore, this method can be used for express primary thickness analyses, including combined coatings, based on transmission spectroscopy results. For the non-ordered aluminum oxide film with the smallest pore diameter, the discrepancy between the thickness calculation results was more than one and a half times, but the refractive index value is comparable to the value

for amorphous PAAO [46]. This result could be associated with the peculiarities of the propagation of radiation in the quasi-periodic oxide structure, especially by two- and manyfold reflections combined with scattering on alumina defects.

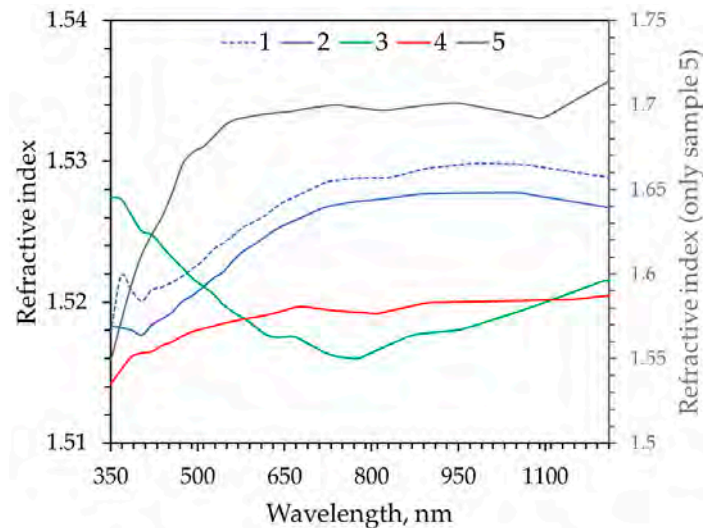The dispersion of the refractive index was estimated in the wavelength region of 350–1200 nm (Figure 7).

Figure 7. Dispersion of refractive indices of the valve metals functional thin films.

For all quasi-ordered samples, the average refractive index is about 1.52 ± 0.01 and remains stable over the analyzed wavelength range under consideration. These values are lower than usual for PAAO, which suggests that porous anodic films with small thicknesses due to the well-ordered structure of anodic oxides will have a refractive index lower than a transparent substrate, but unlike thicker anodized aluminum coatings, will have good adhesion due to the presence of a sublayer [47–50].

The transmission degree of the synthesized films was estimated through the integral transmission in the visible (VIS), near-infrared (NIR), and near-ultraviolet (NUV) regions and normalized to the degree of glass transmission using the equation:

$$T_N = (T/T_0) \times 100\%,\qquad(4)$$

where T_N is the sample transmission and T_0 is the glass transmission.

The results of the transmission analysis are represented in Figure 8.
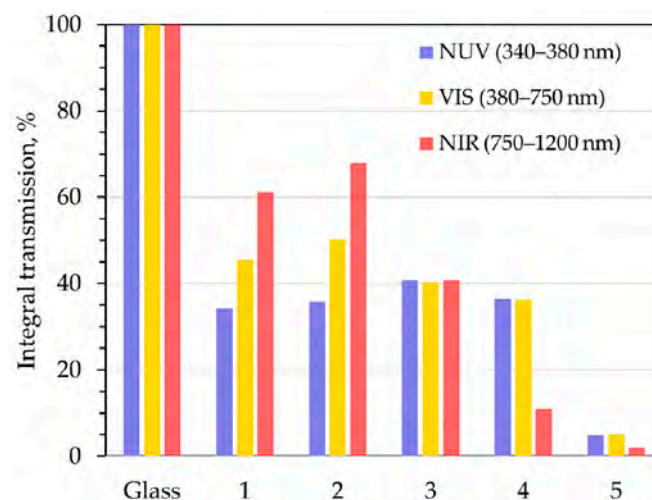

Figure 8. Normalized integral transmission of the valve metals functional thin films.

On average, the transmission attenuation for quasi-ordered samples 1–4 in the ranges studied is about 40–60%. The best transmittance is recorded in the NIR range for anodic aluminum films containing a sublayer of tantalum. Such optical properties and the possibility of incorporating PAAO-based structures with the luminescent ions by sol–gel synthesis and dipping make Al/Ta oxide structures promising for use as IR transparent window materials, emitting devices, transparent radiation converters, and for IR-spectroscopy of catalytic reactions without submersible manipulators. UV attenuation can be useful for operation with film organic–inorganic solar cells to slow down their degradation [50–53]. The integration of magnetic nanoparticles into pores of semi-transparent oxide has potential for applications such as electromagnetic interference shielding and magneto-optical storage with cheaper technology, excluding the existing deficiencies of using polymer matrices [54]. The slight improvement of transmission in all wavelength ranges after additional heat treatment at 450 °C for aluminum oxide films on a sublayer of tantalum oxide may be due to the final removal of water and organic compounds from the oxides. The non-ordered PAAO film obtained by anodizing in a mixture of sulfuric and oxalic acids at 20 V shows the worst transmission, associated with the low ordering of the resulting oxide at the smallest pore sizes ($\geq$20 nm according to SEM data), which contributes to increased scattering and repeated reflection and absorption of optical radiation in the thickness of the oxide throughout the wavelength range. PAAO with a sublayer of vanadium oxide is characterized by the uniform transmission of radiation over the entire wavelength range.

4. Conclusions

Novel semi-transparent multilayered valve metals oxide coatings on glass substrates, obtained by electrochemical oxidation in potentiostatic mode in the oxalic electrolyte at 60 V from the sputtered Al, V, and Ta thin films were proposed. PAAO was formed by one-step anodizing on Ta or V oxide sublayers in quasi-ordered and non-ordered (in the sulfuric–oxalic electrolyte at 20 V) forms, which was confirmed by SEM analysis. Transmission spectroscopy confirmed the main role of the PAAO ordering process in the transparent properties of the obtained layered structures.

All samples, excluding non-ordered PAAO obtained in the sulfuric–oxalic electrolyte at 20 V, demonstrate semi-transparentness in the range of 300–2800 nm. The refractive index, obtained by the envelope method from transmission spectra, for the sample with non-ordered PAAO demonstrates about 1.70 ± 0.01 in the range of 500–1200 nm and exponential damping in the range of 300–500 nm, while samples with quasi-ordered PAAO have refractive indices of 1.52 ± 0.01 in the full range of 300–1200 nm.

Non-ordered PAAO is almost non-transparent in the range of 340–1200 nm—the integral transmission is less than 8%. Quasi-ordering PAAO increases the integral transmission 6–7 times in the NUV and 6–10 times in the visible areas, and also up to 7.5 times in the NIR area. Adding sublayers of vanadium or tantalum oxides for quasi-ordered PAAO decreases the integral transmission in the range of 340–1200 nm with a maximal effect of 35% for the NUV area and up to 6 times in the NIR area, according to the differences in the structure of the intermediate sublayer between PAAO and glass.

Thus, thin layers of Al_2O_3 on glass can be used for different applications depending on their characteristics. Adding sublayers of vanadium or tantalum oxides allows changes in transparency, especially in the NUV area for the Al/Ta films, and monoxide aluminum layers can be useful for developing semi-transparent coatings with an attenuation intensity of NUV radiation. Moreover, these coatings are promising for the subsequent forming of photocatalytic and luminescent/up-conversion thin films, which can be activated from both sides.

References

1. Saji, V.S. Superhydrophobic surfaces and coatings by electrochemical anodic oxidation and plasma electrolytic oxidation. *Adv. Colloid Interface Sci.* **2020**, *283*, 102245. [CrossRef] [PubMed]
2. Azadian, F.; Rastogi, A.C. Energy storage performance of thin film nanocrystalline vanadium oxide with fluorinated tin oxide current carrier electrode for solid-state transparent supercapacitors based on ionic liquid gel electrolyte. *Electrochim. Acta* **2019**, *330*, 135339. [CrossRef]
3. Khoroshko, L.S.; Kortov, V.S.; Gaponenko, N.V.; Raichyonok, T.F.; Tikhomirov, S.A.; Pustovarov, V.A. X-ray-, cathodo-, and photoluminescence of yttrium–aluminum composites on porous anodic alumina films. *J. Appl. Spectrosc.* **2016**, *83*, 358–361. [CrossRef]
4. Khoroshko, L.S. Two-dimensional porous anodic alumina for optoelectronics and photocatalytic application. *J. Phys. Conf. Ser.* **2015**, *643*, 012110. [CrossRef]
5. Yoldas, B.E. Investigations of porous oxides as an antireflective coating for glass surfaces. *Appl. Opt.* **1980**, *19*, 1425–1429. [CrossRef]
6. Petrovykh, K.A.; Kortov, V.S.; Gaponenko, N.V.; Rempel', A.A.; Rudenko, M.V.; Khoroshko, L.S.; Voznesenskii, S.S.; Sergeev, A.A.; Pustovarov, V.A. Photoluminescence of the nanosized xerogel Zn_2SiO_4:Mn^{2+} in pores of anodic alumina. *Phys. Solid State* **2016**, *58*, 2062–2067. [CrossRef]
7. Korzhik, M.V. On the limit of the accuracy of time stamp at the detection of annihilation g-quanta with a scintillation detector. *J. BSU Phys.* **2021**, *2*, 96–101. [CrossRef]
8. Wilcox, P.S.; Westwood, W.D. Anodic Oxidation of Tantalum. *Can. J. Phys.* **1976**, *49*, 1543–1548. [CrossRef]
9. Lee, H.; Kumbhar, V.S.; Lee, J.; Choi, Y.; Lee, K. Highly reversible crystal transformation of anodized porous V_2O_5 nanostructures for wide potential window high-performance supercapacitors. *Electrochim. Acta* **2020**, *334*, 135618. [CrossRef]
10. Gies, M.; Rempel, T.; Becker, M.; Polity, A. Advantageous optical characteristics of tantalum vanadium oxide as counter electrode in electrochromic devices. *J. Mater. Sci.* **2022**, *57*, 12810–12823. [CrossRef]
11. Fialho, L.; Almeida Alves, C.F.; Marques, L.S.; Carvalho, S. Development of stacked porous tantalum oxide layers by anodization. *Appl. Surf. Sci.* **2020**, *511*, 145542. [CrossRef]
12. McQuaig, M.K.; Toro, A.; Van Geertruyden, W.; Misiolek, W.Z. The effect of high temperature heat treatment on the structure and properties of anodic aluminum oxide. *J. Mater. Sci.* **2011**, *46*, 243–253. [CrossRef]
13. Chu, S.Z.; Wada, K.; Inoue, S.; Todoroki, S. Formation and Microstructures of Anodic Alumina Films from Aluminum Sputtered on Glass Substrate. *J. Electrochem. Soc.* **2002**, *149*, B321. [CrossRef]
14. Chu, S.Z.; Wada, K.; Inoue, S.; Todoroki, S. Fabrication and characteristics of nanostructures on glass by Al anodization and electrodeposition. *Electrochim. Acta* **2003**, *48*, 3147–3153. [CrossRef]
15. Chernyakova, K.; Vrublevsky, I.; Jagminas, A.; Klimas, V. Effect of anodic oxygen evolution on cell morphology of sulfuric acid anodic alumina films. *J. Solid State Electrochem.* **2021**, *25*, 1453–1460. [CrossRef]
16. Peitao, G.; Zhilin, X.; Yiyu, X.; Caihu, H.; Lixin, Z. Morphology and transmittance of porous alumina on glass substrate. *Appl. Surf. Sci.* **2011**, *257*, 3307–3312. [CrossRef]
17. Chu, S.Z.; Wada, K.; Inoue, S.; Todoroki, S. Fabrication of oxide nanostructures on glass by aluminum anodization and sol–gel process. *Surf. Coat. Tech.* **2003**, *169–170*, 190–194. [CrossRef]
18. Gapusan, R.B.; Mones, E.S.; Vasquez, M.R. Fabrication of transparent conducting aluminum thin film via anodization-etching of thermally evaporated aluminum on glass. *AIP Conf. Proceed.* **2021**, *2382*, 020008.

19. Rabin, O.; Herz, P.R.; Lin, Y.-M.; Akinwande, A.I.; Cronin, S.B.; Dresselhaus, M.S. Formation of Thick Porous Anodic Alumina Films and Nanowire Arrays on Silicon Wafers and Glass. *Adv. Funct. Mater.* **2003**, *13*, 631–638. [CrossRef]
20. Foong, T.R.B.; Sellinger, A.; Hu, X. Origin of the Bottlenecks in Preparing Anodized Aluminum Oxide (AAO) Templates on ITO Glass. *ACS Nano* **2008**, *2*, 2250–2256. [CrossRef]
21. Taheriniya, S.; Parhizgar, S.S.; Sari, A.H. Investigating the effect of sputtering conditions on the physical properties of aluminum thin film and the resulting alumina template. *Res. Phys.* **2018**, *9*, 1428–1435. [CrossRef]
22. Fan, D.; Ding, G.; Shen, W.; Zheng, M. Anion impurities in porous alumina membranes: Existence and functionality. *Microporous Mesoporous Mater.* **2007**, *100*, 154–159. [CrossRef]
23. Yang, Y.; Gao, Q. Influence of sulfosalicylic acid in the electrolyte on the optical properties of porous anodic alumina membranes. *Phys. Lett. A* **2004**, *333*, 328–333. [CrossRef]
24. Xu, W.; Chen, H.; Zheng, M.; Ding, G.; Shen, W. Optical transmission spectra of ordered porous alumina membranes with different thicknesses and porosities. *Opt. Mater.* **2006**, *28*, 1160–1165. [CrossRef]
25. Jeon, C.; Kim, D.; Lee, Y.; Han, J.; Choi, Y.; Bu, S.; Shin, H.; Yoon, S. Strong pore-size dependence of the optical properties in porous alumina membranes. *J. Korean Phys. Soc.* **2013**, *63*, 1789–1793. [CrossRef]
26. Choudhari, K.; Kulkarni, S.D.; Unnikrishnan, V.; Sinha, R.K.; Santhosh, C.; George, S.D. Optical characterizations of nanoporous anodic alumina for thickness measurements using interference oscillations. *Nano-Struct. Nano-Obj.* **2019**, *19*, 100354. [CrossRef]
27. Podhorodecki, A.; Gaponenko, N.V.; Zatryb, G.; Molchan, I.S.; Motyka, M.; Serafinczuk, J.; Golacki, L.W.; Khoroshko, L.S.; Misiewicz, J.; Thompson, G.E. Ion–ion interaction in two-dimensional nanoporous alumina filled with cubic $YAlO_3$: Tb^{3+} matrix. *J. Phys. D Appl. Phys.* **2013**, *46*, 355302. [CrossRef]
28. Choudhari, K.S.; Choi, C.-H.; Chidangil, S.; George, S.D. Recent Progress in the Fabrication and Optical Properties of Nanoporous Anodic Alumina. *Nanomaterials* **2022**, *12*, 444. [CrossRef]
29. Golovan', L.A.; Kashkarov, P.K.; Timoshenko, V.Y. Form birefringence in porous semiconductors and dielectrics: A review. *Crystallogr. Rep.* **2007**, *52*, 672–685. [CrossRef]
30. Huang, K.; Li, Y.; Wu, Z.; Li, C.; Lai, H.; Kang, J. Asymmetric light reflectance effect in AAO on glass. *Opt. Express* **2011**, *19*, 1301–1309. [CrossRef]
31. Tishkevich, D.I.; Vorobjova, A.I.; Bondaruk, A.A.; Dashkevich, E.S.; Shimanovich, D.L.; Razanau, I.U.; Zubar, T.I.; Yakimchuk, D.V.; Dong, M.G.; Sayyed, M.I.; et al. The Interrelation of Synthesis Conditions and Wettability Properties of the Porous Anodic Alumina Membranes. *Nanomaterials* **2022**, *12*, 2382. [CrossRef] [PubMed]
32. Vorobjova, A.A.; Vorobjova, A.I.; Tishkevich, D.I.; Outkina, E.A.; Shimanovich, D.L.; Razanau, I.U.; Zubar, T.I.; Bondaruk, A.A.; Zheleznova, E.K.; Dong, M.; et al. A Study of Ta_2O_5 Nanopillars with Ni Tips Prepared by Porous Anodic Alumina through-Mask Anodization. *Nanomaterials* **2022**, *12*, 1344. [CrossRef] [PubMed]
33. Vorobjova, A.; Tishkevich, D.; Shimanovich, D.; Zubar, T.; Astapovich, K.; Kozlovskiy, A.; Zdorovets, M.; Zhaludkevich, A.; Lyakhov, D.; Michels, D.; et al. The influence of the synthesis conditions on the magnetic behavior of the densely packed arrays of Ni nanowires in porous anodic alumina membranes. *RSC Adv.* **2021**, *11*, 3952–3962. [CrossRef] [PubMed]
34. Tishkevich, D.I.; Vorobjova, A.I.; Vinnik, D.A. Formation and corrosion behavior of Nickel/Alumina nanocomposites. *Solid State Phenom.* **2020**, *299*, 100–106. [CrossRef]
35. Vorobjova, A.I.; Shimanovich, D.L.; Sycheva, O.A.; Ezovitova, T.I.; Tishkevich, D.I.; Trykhanov, A.V. Studying the Thermodynamic Properties of Composite Magnetic Material Based on Anodic Alumina. *Russ. Microelectron.* **2019**, *48*, 107–118. [CrossRef]
36. Tishkevich, D.; Vorobjova, A.; Shimanovich, D.; Kaniukov, E.; Kozlovskiy, A.; Zdorovets, M.; Vinnik, D.; Turutin, A.; Kubasov, I.; Kislyuk, A.; et al. Magnetic Properties of the Densely Packed Ultra-Long Ni Nanowires Encapsulated in Alumina Membrane. *Nanomaterials* **2021**, *11*, 1775. [CrossRef]
37. Tishkevich, D.I.; Vorobjova, A.I.; Trukhanov, A.V. Thermal stability of nano-crystalline nickel electrodeposited into porous alumina. *Solid State Phenom.* **2020**, *299*, 281–286. [CrossRef]
38. Tishkevich, D.I.; Vorobjova, A.I.; Vinnik, D.A. Template Assisted Ni Nanowires Fabrication. *Mater. Sci. Forum* **2019**, *946*, 235–241. [CrossRef]
39. Tishkevich, D.I.; Vorobjova, A.I.; Shimanovich, D.L.; Vinnik, D.A.; Zubar, T.I.; Kozlovskiy, A.L.; Zdorovets, M.V.; Yakimchuk, D.V.; Trukhanov, S.V.; Trukhanov, A.V. Formation and corrosion properties of Ni-based composite material in the anodic alumina porous matrix. *J. Alloys Compd.* **2019**, *804*, 139–146. [CrossRef]
40. Vorobjova, A.I.; Tishkevich, D.; Shimanovich, D.; Zdorovets, M. Electrochemical Behaviour of $Ti/Al_2O_3/Ni$ Nanocomposite Material in Artificial Physiological Solution: Prospects for Biomedical Application. *Nanomaterials* **2020**, *10*, 173. [CrossRef]
41. Shimanovich, D.L.; Vorobjova, A.I.; Tishkevich, D.I. Preparation and morphology-dependent wettability of porous alumina membranes. *Beilstein J. Nanotechnol.* **2018**, *9*, 1423–1436. [CrossRef]
42. Kushwaha, M.K. A comparative Study of Different Electrolytes for Obtaining Thick and Well-ordered nano-porous Anodic Aluminium Oxide (AAO) Films. *Proc. Mater. Sci.* **2014**, *5*, 1266–1273. [CrossRef]
43. Myung, N.V.; Lim, J.; Fleurial, J.-P.; Yun, M.; West, W.; Choi, D. Alumina nanotemplate fabrication on silicon substrate. *Nanotechnology* **2004**, *15*, 833–838. [CrossRef]
44. Swanepoel, R. Determination of the thickness and optical constants of amorphous silicon. *J. Phys. E Sci. Instrum.* **1983**, *16*, 1214–1222. [CrossRef]

45. Sánchez-González, J.; Díaz-Parralejo, A.; Ortiz, A.L.; Guiberteau, F. Determination of optical properties in nanostructured thin films using the Swanepoel method. *Appl. Surf. Sci.* **2006**, *252*, 6013–6017. [CrossRef]

46. Yamaguchi, A.; Hotta, K.; Teramae, N. Optical Waveguide Sensor Based on a Porous Anodic Alumina/Aluminum Multilayer Film. *Anal. Chem.* **2009**, *81*, 105–111. [CrossRef] [PubMed]

47. Gervais, F. *Handbook of Optical Constants of Solids II*; Palik, E.D., Ed.; Academic Press, Inc.: Orlando, FL, USA, 1991; pp. 761–775.

48. Chen, J.; Wang, B.; Yang, Y.; Shi, Y.; Xu, G.; Cui, P. Porous anodic alumina with low refractive index for broadband graded-index antireflection coatings. *Appl. Opt.* **2012**, *51*, 6839–6843. [CrossRef] [PubMed]

49. Liu, X.J.; Chen, F.; Zhang, F.; Zhang, H.L.; Zhang, Z.; Wang, J.; Wang, S.W.; Huang, Z.R. Hard transparent AlON ceramic for visible/IR windows. *Int. J. Refract. Met. Hard Mater.* **2013**, *39*, 38–43. [CrossRef]

50. Bousslama, W.; Sieber, B.; Elhouichet, H.; Gelloz, B.; Addad, A.; Férid, M. Enhancement of the intensity ratio of ultraviolet to visible luminescence with increased excitation in ZnO nanoparticles deposited on porous anodic alumina. *J. Phys. D Appl. Phys.* **2013**, *46*, 505104. [CrossRef]

51. Stepanova, L.S.; Orekhovskaya, T.I.; Gaponenko, N.V.; Prislopski, S.Y. Terbium luminescence deposited from solution of terbium nitrate on porous anodic alumina. *Dokl. BGUIR* **2010**, *6*, 85–89.

52. Vimont, A.; Thibault-Starzyk, F.; Daturi, M. Analysing and understanding the active site by IR spectroscopy. *Chem. Soc. Rev.* **2010**, *39*, 4928–4950. [CrossRef] [PubMed]

53. Mahon, N.S.; Zelenyak, T.Y.; Korolik, O.V.; Gladyshev, P.P.; Mazanik, A.V. Influence of pyridine treatment on the optical properties of organic-inorganic perovskite films. *J. BSU Phys.* **2019**, *2*, 66–72. [CrossRef]

54. Althues, H.; Henle, J.; Kaskel, S. Functional inorganic nanofillers for transparent polymers. *Chem. Soc. Rev.* **2007**, *36*, 1454–1465. [CrossRef] [PubMed]